THE JOURNAL OF PHYSICAL CHEMISTRY C

Subscriber access provided by KIT Library

C: Surfaces, Interfaces, Porous Materials, and Catalysis

CuPd Mixed-Metal HKUST-1 as Catalyst for Aerobic Alcohol Oxidation

Penghu Guo, Christian Froese, Qi Fu, Yen-Ting Chen, Baoxiang Peng, Wolfgang Kleist, Roland A. Fischer, Martin Muhler, and Yuemin Wang

J. Phys. Chem. C, **Just Accepted Manuscript** • Publication Date (Web): 23 Aug 2018

CuPd Mixed-Metal HKUST-1 as Catalyst for Aerobic Alcohol Oxidation

Penghu Guo,[†] Christian Froese,[†,‡] Qi Fu,[†] Yen-Ting Chen,[†] Baoxiang Peng,*[,†,‡] Wolfgang Kleist,[†] Roland A. Fischer,[§] Martin Muhler,*[,†,‡] Yuemin Wang*[,∥]

[†]Laboratory of Industrial Chemistry, Ruhr-University Bochum, 44780 Bochum, Germany

[‡]Max Planck Institute for Chemical Energy Conversion, 45470 Mülheim an der Ruhr, Germany

[§]Chair of Inorganic and Metal-Organic Chemistry Department of Chemistry, Technical University of Munich, 85748 Garching, Germany.

[∥]Institute of Functional Interfaces, Karlsruhe Institute of Technology, 76344 Eggenstein-Leopoldshafen, Germany.

ABSTRACT

Metal-organic frameworks (MOFs) featuring isolated coordinatively unsaturated metal sites (CUS) have enormous potential as single-site catalysts. In particular, mixed-metal MOFs may exhibit unique catalytic properties compared to their monometallic counterparts. Herein, we report a thorough fundamental study on the mixed-metal CuPd-HKUST-1 ($[Cu_{3-x}Pd_x(BTC)_2]_n$; BTC = 1,3,5-benzenetricarboxylate) including the two-step synthesis, characterization and catalytic performance evaluation. The combined results from a multi-technique approach provide solid evidence that the chemical properties of HKUST-1 can be tuned via successful incorporation of Pd-CUS into the framework leading to the formation of new Cu-Pd and/or Pd-Pd dimers. The introduction of Pd occurs exclusively at the metal nodes in a controlled manner while retaining the structural integrity. All the incorporated Pd ions have an oxidation state of +2 whereas no PdO or metallic Pd nanoparticles embedded inside MOFs are detected. These mixed-metal CuPd-MOFs exhibit superior catalytic activity and selectivity for the aerobic oxidation of benzyl alcohol to benzaldehyde, and the doped Pd^{2+}-CUS species are identified as isolated single active sites.

1 INTRODUCTION

Metal-organic-frameworks (MOFs) featuring novel physical and chemical properties have opened up new perspectives in numerous application fields ranging from gas/liquid storage and separation, chemical sensing, drug release to electronic devices and catalysis.[1-6] Their high structural and compositional design flexibility, which can be implemented by guest inclusion, solvent-assisted linker exchange, varying organic linker with different structure and coordination modes as well as by defect-engineering, allows to precisely tailor MOF materials for specific targeted applications. [7-30] In heterogeneous catalysis, the special interest in MOFs results from the presence of coordinatively unsaturated metal sites (CUS) at the framework nodes which act as isolated single active sites.[31,32]

The Cu-based HKUST-1 ($[Cu_3(BTC)_2]$; BTC = 1,3,5-benzenetricarboxylate) is a prototypical MOF and contains copper-carboxylate paddle-wheel building units exposing intrinsic undercoordinated Cu^{2+} sites (Cu-CUS, see Figure 1),[33] which show catalytic activity for a variety of reactions, such as α-pinene oxide rearrangement, acetalization of aldehydes with methanol and quinoline synthesis.[34-38] Recently, it has been reported that the chemical and physical properties of MOF materials can be tuned by modification of both organic linkers and metal nodes.[15-30] The defect-engineered MOFs (DEMOFs) formed via the incorporation of defect linkers or different metal ions are expected to show improved catalytic activity with respect to the pristine MOFs. However, a thorough atomic-level understanding of DEMOFs remains still a major challenge due to the great structural complexity. In particular, there is little information available on mixed-metal MOFs produced by the strategy of metal node engineering.[39-45]

The controlled integration of Pd^{2+} cations into the metal nodes of HKUST-1 yielding CuPd mixed-metal single-sites is of great interest with regard to the unique catalytic performance of

palladium compounds for many reactions such as alcohol oxidation, allylic oxidation/rearrangements, olefin hydrogenation and cycloisomerization.[46-52] Llabrés i Xamena et al.[53] have reported that the monometallic Pd-MOF with the molecular formula $[Pd(2\text{-pymo})_2]_n$ (2-pymo = 2-hydroxypyrimidinolate) is active for typical Pd-catalyzed reactions. Although Pd^{2+} possesses a similar effective ionic radius as Cu^{2+}, the synthesis of CuPd mixed-metal HKUST-1 is a challenging task due to the difficulties in crystallizing 3D structures caused by kinetic reasons.[54] Recently, $Pd^0@[(Cu_{3-x}Pd_x(BTC)_2]_n$ was synthesized via one-pot hydrothermal method, leading to the coexistence of both Pd^{2+}-CUS at the framework nodes and Pd^0 NPs embedded inside MOFs.[54] However, the exclusive introduction of Pd^{2+} as framework nodes has not yet been achieved.

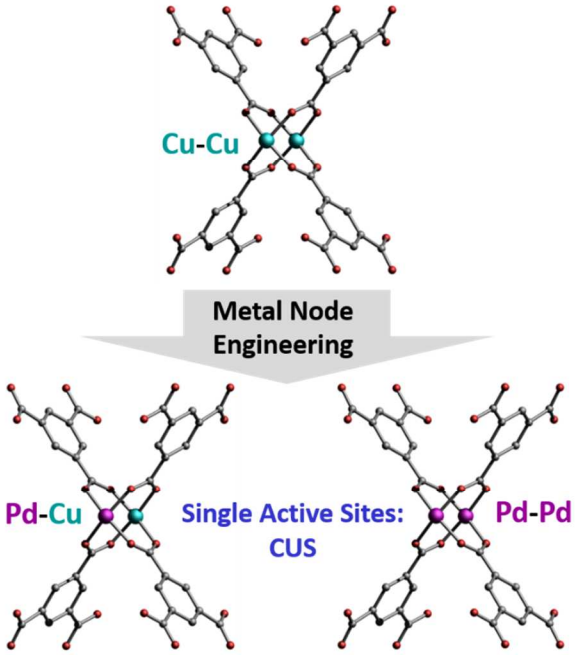

Figure 1. CuPd mixed-metal HKUST-1 synthesized using the strategy of metal node engineering.

Here, we report a novel two-step synthesis that enables to produce mixed-metal $[Cu_{3-x}Pd_x(BTC)_2]_n$ (CuPd-HKUST-1) with controllable modification exclusively at the metal nodes, giving rise to Cu-Pd and/or Pd-Pd paddlewheels (Figure 1). The successful homogeneous incorporation of Pd^{2+} is confirmed by a comprehensive multi-technique study. Our results reveal that the mixed-metal CuPd-MOF exhibits superior catalytic performance compared to the pristine HKUST-1 for the selective aerobic oxidation of benzyl alcohol to benzaldehyde. The improved reactivity and selectivity are attributed to the presence of doped Pd^{2+} CUS, acting as isolated single active sites.

2. Experimental

2.1 Materials. All reagents used in the experiment were purchased from Sigma-Aldrich and used as received without further purification.

2.1.1 Synthesis of Compound 1. $Cu(NO_3)_2 \cdot 3H_2O$ (0.288 g, 1.19 mmol) and $Pd(OAc)_2$ (0.047 g, 0.21 mmol) were loaded into a 25 mL glass bottle followed by adding 6 mL DMF (HPLC grade) immediately, and then the mixture was stirred vigorously to completely dissolve all metal salts at room temperature for 1 hour obtaining solution A. Ligand H_3BTC (0.198 g, 0.94 mmol) was dissolved in 6 mL DMF in another 25 mL glass bottle to obtain solution B, which was then added to the solution A under continuous stirring condition for 1 hour. Subsequently, the mixed solution in the glass bottle was sealed and placed into a preheated oven at 343 K for 12 h. Afterwards, the bottle was taken out and cooled down to room temperature naturally. The raw product was collected by centrifugation and then washed by DMF several times to remove the unreacted precursors. This raw product was then soaked in DMF and kept in oven at 323 K for 3 hours. Finally, the raw product was obtained by centrifugation followed by solvent

exchange with acetone (HPLC grade) every 6 h for 6 times (7 mL each time). The yield is around 45% for compound **1**. Before further measurements, the sample was activated by heating at certain temperature for 4 h under dynamic vacuum (around 10^{-2} mbar).

2.1.2. Synthesis of Compound 2. All procedures are similar with the synthesis of compound **1** except the amount of metal precursors, that is, $Cu(NO_3)_2 \cdot 3H_2O$ (0.184 g, 0.98 mmol) and $Pd(OAc)_2$ (0.094 g, 0.42 mmol). The yield for compound **2** is slightly higher, around 50%.

2.1.3 Synthesis of Pristine HKUST-1. $Cu(NO_3)_2 \cdot 3H_2O$ (0.338 g, 1.4 mmol) and H_3BTC (0.200 g, 0.94 mmol) were loaded into a 25 mL glass bottle and then 12 mL DMF (HPLC grade) was added. After vigorously stirring for 1 h, the glass bottle was sealed and placed into a preheated oven at 343 K for 24 h. Afterwards, the bottle was taken out from oven and cooled down naturally to room temperature. The resulting solid was collected by centrifugation followed by solvent washing with ethanol, H_2O and acetone. The yield is around 55%.

2.2. Characterization. The samples were identified by powder XRD over the 2θ range 4 - 60° with Cu Kα radiation and scan step 0.01313°. HR-XPS was performed using an ultra-high vacuum setup equipped with a high resolution Gammadata Scienta SES 2002 analyser. The spectra were obtained at pass energy 200 eV with a base pressure around 3×10^{-10} mbar and an analyzer slit width of 0.3 mm. Monochromatic Al Kα (1486.6 eV) was used as incident radiation. Energy resolution is better than 0.5 eV and flood gun is used to compensate for charging effects. All spectra were calibrated to C1s binding energy at 284.5 eV. The analysis of the spectra was performed using CasaXPS software with mixed Gaussian-Lorentzian function and Shirley background subtraction. For UHV-FTIR spectra, samples were pressed into a stainless steel grid covered by gold and then was mounted on the sample holder, which was

specially designed for the UHV-FTIR transmission measurement.[55,56] Base pressure in the measurement chamber was 8×10^{-10} mbar. Before measurement, sample was heated at 393 K to remove all adsorbed chemical species. CO dosing was carried out by backfilling the measurement chamber through a leak valve. Spectra were collected with 512 scans and 4 cm^{-1} resolution. TEM and EDS elemental mapping measurement were conducted by JEM-2800, JEOL setup with beam energy 200 kV. The effective area of detector is 200 mm^2. Resolution is 0.09 nm and 123 eV for TEM and EDS, respectively. BET surface area and pore size distribution were measured by N_2 physisorption at 77 K using BelMax sorption machine from BelJapan. Samples were activated at 393 K for 4 h before measurement. TG measurements were carried out on a thermo balance with a coupled QMS under helium condition. Heating ramp was 2 K min^{-1} until final temperature 723 K.

2.3. Catalytic Oxidation. The aerobic oxidation of benzyl alcohol was conducted in a 100 mL Parr autoclave. The catalysts were pre-activated at indicated temperatures (393 K, 423 K, 443 K, 473 K) for 6 h under dynamic vacuum conditions (~10^{-2} mbar). The heating ramp was set to 5 K min^{-1}. In a typical run, 96 µL benzyl alcohol, 20 mL toluene as solvent, and 100 mg pre-activated catalyst were loaded into the reactor followed by purging with oxygen for three times. The reactor was then pressurized with 5 bar oxygen and heated to 403 K with a stirring speed of 700 rpm. During reaction, around 1 mL liquid sample was taken out from the reactor through sampling line at appropriate intervals. The solution was centrifuged and then analyzed by gas chromatography.

The samples were analyzed by an Agilent 7820A gas chromatography equipped with a capillary column (ZB-WAXplus, 30 m × 0.32 µm × 0.25 µm), a flame ionization detector (FID), and an autosampler. The GC was calibrated using several mixed solution with different concentrations

to obtain response factor for each compound. The conversion of benzyl alcohol as well as the selectivity and yield of products were calculated based on normalization.

3. RESULTS and DISCUSSION

3.1. Synthesis and Characterization of Mixed-Metal CuPd-MOFs. We synthesized the mixed-metal CuPd-HKUST-1 ($[Cu_{3-x}Pd_x(BTC)_2]_n$) by using a novel two-step approach, in which a mixed-metal ion (Cu^{2+} and Pd^{2+}) solution in dimethylformamide (DMF) was prepared first, and H_3BTC dissolved in DMF was then added under continuous stirring. The solution was kept in an oven at 343 K for 12 h and then cooled to room temperature to obtain the desired samples. During the synthesis, we utilized DMF instead of common aqueous alcohol solutions, thus avoiding the coexistence of metallic Pd^0 nanoparticles (NPs) that could be formed via the reduction of Pd^{2+} ions by alcohols at elevated temperatures.

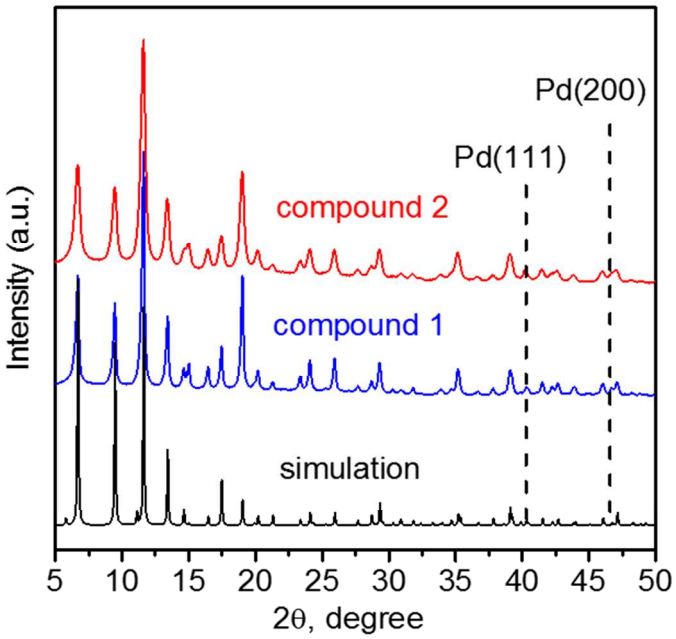

Figure 2. Powder XRD patterns of CuPd mixed-metal MOFs (compounds **1** and **2)** and simulated pattern of pristine HKUST-1.

The phase purity of the synthesized samples, $[Cu_{2.43}Pd_{0.57}(BTC)_2]_n$ (**1**) and $[Cu_{1.77}Pd_{1.23}(BTC)_2]_n$ (**2**), was demonstrated by powder X-ray diffraction (XRD) data. As shown in Figure 2, the XRD patterns match well with the simulated pristine HKUST-1, indicating the same framework and the preserved structural integrity after the introduction of Pd^{2+}. The increasing Pd^{2+} doping level leads to slight broadening of the reflections, which is probably attributed to a lower degree of crystallinity and the distortion of crystal lattice caused by the partial substitution of metal nodes. It should be noted that compared with the simulated pattern, no additional reflections at about 40.2° and 46.7° due to Pd(111) and Pd(200) were observed for compounds **1** and **2**, thus excluding the presence of metallic Pd in both samples.

Thermogravimetric analysis (TGA) revealed that the decomposition of both CuPd mixed-metal HKUST-1 samples occurs at ~ 523 K (see Figure S1). The XRD patterns of compound **2** obtained before and after activation at 393 K as well as after catalytic reaction confirmed again the thermal stability of the framework (Figure S2).

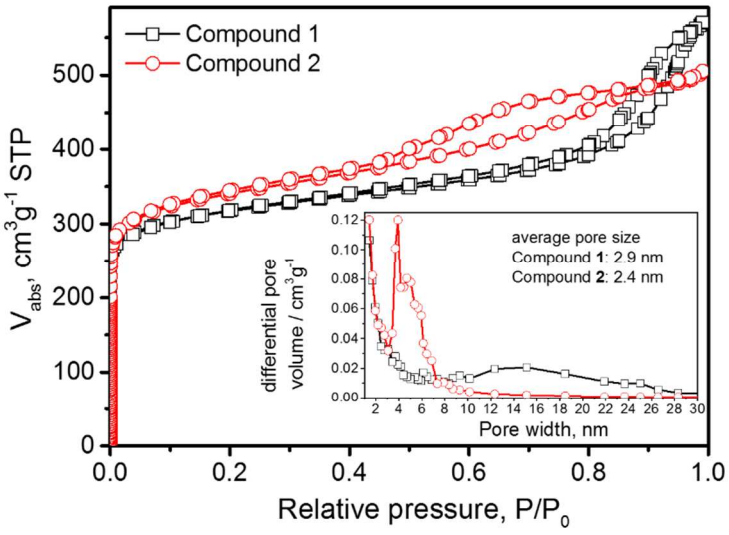

Figure 3. N_2 physisorption isotherms and pore size distributions (inset) for CuPd mixed-metal MOFs (compounds **1** and **2)**. Both samples were activated at 393 K under vacuum to completely remove adsorbed species prior to the measurement.

To further support the incorporation of Pd^{2+} ions into the framework nodes, we carried out N_2 adsorption-desporption experiments at 77 K. Both CuPd mixed metal MOFs (**1** and **2**) show the type IV N_2 physisorption isotherms (see Figure 3), suggesting the presence of micropores and mesopores. Hierarchical porosity distribution is illustrated in the inset of Figure 3, and the average pore sizes are around 2.9 and 2.4 nm for compounds **1** and **2**, respectively. The mesopores presumably originate from defects (e.g. missing paddlewheels) created by the acetate modulator (CH_3COO^-), and they are expected to facilitate diffusion of reactants and products (*i.e.*, benzyl alcohol, benzaldehyde and benzoic acid) to or from the metal-CUSs.[12-15] Total pore volumes were determined to amount to 0.88 cm^3 g^{-1} for **1** and 0.78 cm^3 g^{-1} for **2**. The specific surface areas of both CuPd-MOFs (1206 and 1284 m^2 g^{-1} for **1** and **2,** respectively, derived by

applying the BET equation) are still comparable to the pristine HKUST-1,[57-60] indicating that Pd^{2+} should be located at the metal nodes (*i.e.*, Cu^{2+}-Pd^{2+} and/or Pd^{2+}-Pd^{2+} PWs, see Figure 1), instead of occupying the pores. In addition, the results from TEM-EDS elemental mapping revealed a homogeneous distribution of Cu and Pd components in the framework for both compounds **1** and **2** (Figure 4 and Figure S3), which indicates again the successful incorporation of Pd^{2+} ions into the framework of HKUST-1.

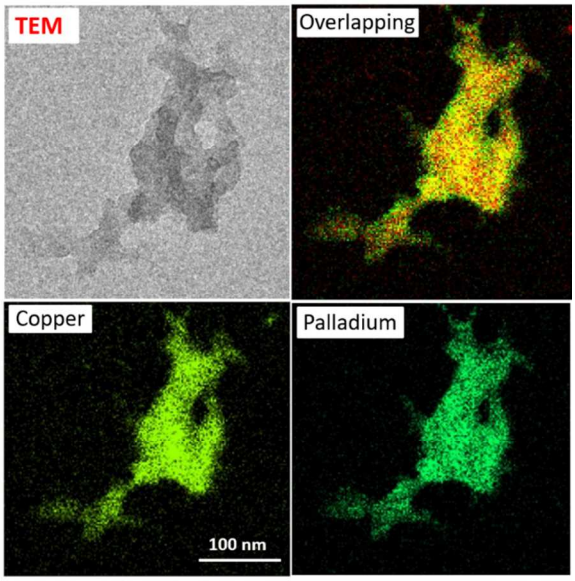

Figure 4. TEM image and EDS metal mapping for CuPd mixed-metal HKUST-1 (compound **2)**.

3.2. XPS and UHV-FTIRS Analysis. The CuPd mixed-metal MOFs (compounds **1** and **2**) were further characterized by high-resolution X-ray photoelectron spectroscopy (HR-XPS) to identify the oxidation states of metal components. The coexistence of palladium and copper in compounds **1** and **2** was verified by the survey scan (Figure S4). Figure 5 presents the deconvoluted Cu 2p and Pd 3d XPS data. The Cu 2p spectra are dominated by the $2p_{3/2}$ peak at 934.7 eV, which is ascribed to the intrinsic Cu^{2+} ions in HKUST-1 as further confirmed by the typical shake-up satellites centered at about 940 and 944 eV. Importantly, the Pd 3d XPS data for

both CuPd-MOFs show only one doublet at 338.3 eV (Pd $3d_{5/2}$) and 343.7 eV (Pd $3d_{3/2}$), matching very well with the characteristic binding energies of Pd^{2+} species,[54,61] demonstrating that all palladium species in the CuPd mixed-metal HKUST-1 are in the oxidation state of +2. This result further supports the conjecture that all Pd^{2+} ions serve as framework nodes (Cu^{2+}-Pd^{2+} and/or Pd^{2+}-Pd^{2+} PWs). A quantitative analysis reveals that the Pd/Cu ratio also increases with increasing Pd^{2+} doping level. The corresponding O 1s spectra showed only one peak at 531.8 eV originating from carboxylate groups in the framework (data not shown), while no indication of the formation of any oxide species was detected. Thus, we can definitely rule out an assignment of the Pd^{2+} species to PdO NPs.

In addition, the deconvolution of the Cu 2p regions reveals the existence of Cu^{+} as minor species in both CuPd-MOFs (Figure 5a), and around 6% and 15% of Cu^{2+} (934.7 eV) are reduced to Cu^{+} (932.4 eV) once activated at 393 K under UHV conditions for compounds **1** and **2**, respectively. For comparison, the XP Cu 2p spectrum of pristine HKUST-1 synthesized by copper nitrate and activated at 393 K was presented in Figure S5, and only around 4% Cu^{+} was observed. These results suggest that the modification of the Cu^{2+} nodes via doping with Pd^{2+} is accompanied by the formation of a small amount of Cu^{+}.

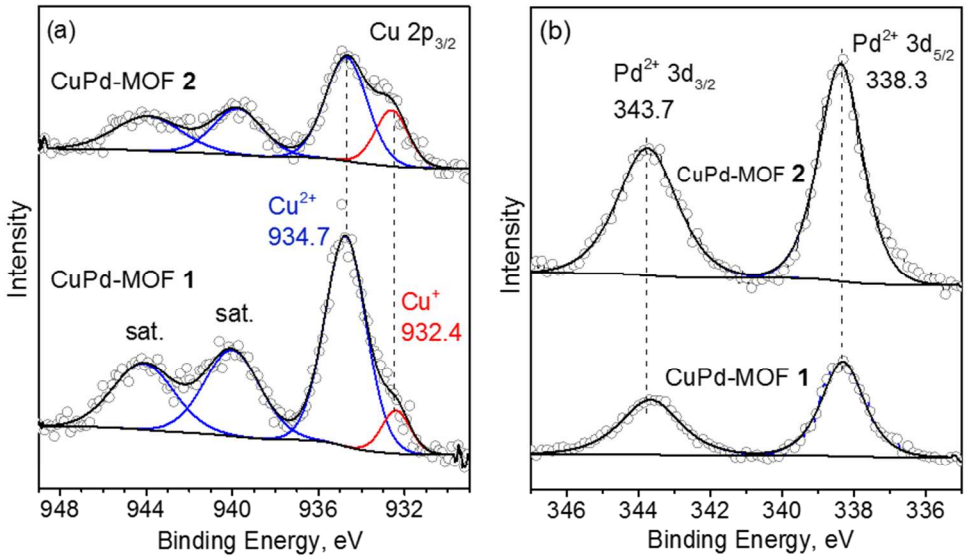

Figure 5. (a) Cu 2p and (b) Pd 3d regions of the deconvoluted XPS data for CuPd mixed-metal MOFs (compounds **1** and **2)** after activation at 393 K.

The chemical nature of Cu- and Pd-CUS sites was further investigated by ultrahigh vacuum Fourier transform infrared spectroscopy (UHV-FTIRS) using CO as a probe molecule (Figure 6). After CO adsorption at 100 K, all three samples (pristine HKUST-1, CuPd-MOFs **1** and **2**) exhibit one sharp dominating band at 2178 cm^{-1} due to Cu^{2+}-CO species. For the pristine Cu-MOF, there are two weak bands at 2118 and 2128 cm^{-1} in the lower-frequency range originating from Cu^{+}-CO species. The redshift in frequency is attributed to the enhanced π back-donation. Given that the extinction coefficient of Cu^{+}-CO is much higher than that of Cu^{2+}-CO,[62] the IR results indicate a very low concentration of intrinsic Cu^{+} defects (a few percent) in the pristine HKUST-1, in line with the XPS results (Figure S5). For CuPd-MOFs **1** and **2**, one new band appears at about 2140 cm^{-1}, and its intensity increases with increasing Pd^{2+} doping level. This band is assigned to Pd^{2+}-CO species, which is consistent with literature.[63] It is known that CO bound to metallic Pd^{0} sites is characterized by vibrational frequencies typically lower than 2100 cm^{-1}. As shown in Figure 6, no any IR bands were observed in the low-frequency region, confirming the absence of additional Pd^{0} NPs embedded in the pore. In addition, the relative concentration of Cu^{+} species increases along with the introduction of Pd^{2+}. These UHV-FTIRS results provide solid evidence for the formation of CuPd mixed-metal HKUST-1 in a controlled manner, in excellent agreement with the XPS observation.

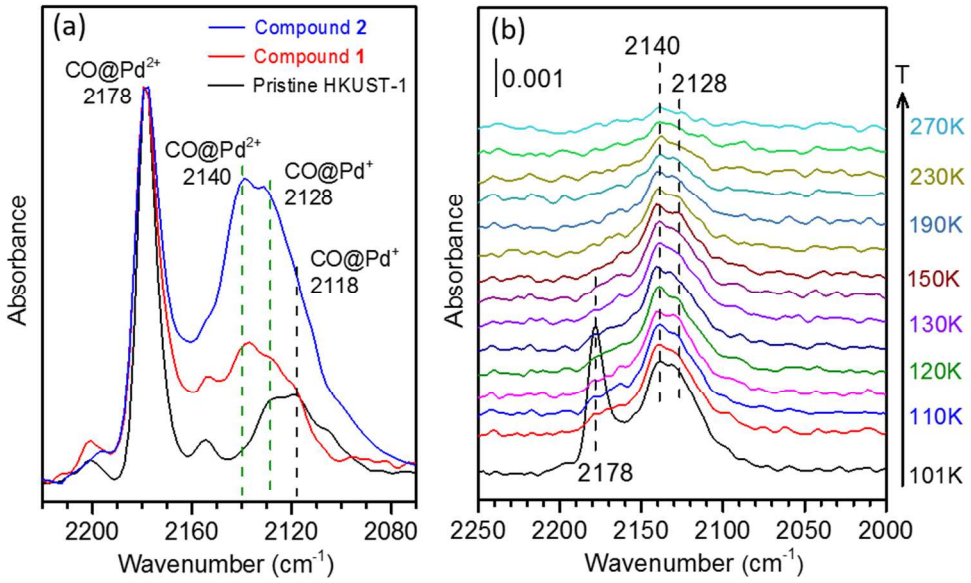

Figure 6. (a) The UHV-FTIR spectra obtained after exposing the pristine HKUST-1 and CuPd mixed-metal MOFs (compounds **1** and **2)** to CO at 100 K. (b) Thermal stability of various CO species adsorbed on CuPd-MOF **2** monitored by temperature-dependent IR spectroscopy. Prior to the measurements, all samples were activated at 393 K to remove adsorbed impurities.

During CO adsorption over CuPd-MOFs **1** and **2** at 100 K, the bands at 2140 cm^{-1} (Pd^{2+}-CO) and 2128 cm^{-1} (Cu^{+}-CO) appear first followed by the main peak at 2178 cm^{-1} (Cu^{2+}-CO) as shown in Figure S6. Furthermore, the thermal desorption of different CO species was investigated by temperature-dependent UHV-FTIRS that allows to gain deeper insight into the interaction between CO and various metal-CUS sites. The major band at 2178 cm^{-1} (Cu^{2+}-CO) disappears first at 115 K followed by the 2128 cm^{-1} band (Cu^{+}-CO) at ~230 K. The band at 2140 cm^{-1} (Pd^{2+}-CO) finally vanishes at about 270 K (Figure 6b). Overall, based on the temperature-dependent FTIR results, the binding energies of CO at different metal-CUS sites follow the sequence $Pd^{2+} > Cu^{+} > Cu^{2+}$.

3.3. Selective Oxidation of Benzyl Alcohol to Benzaldehyde. The aerobic oxidation of alcohols to their corresponding aldehydes or ketones in the liquid phase is an important and promising reaction in organic synthesis. The selective oxidation of benzyl alcohol to benzaldehyde is often used as a probe reaction to assess the catalytic activity of catalysts, and benzaldehyde is the second most important aromatic compound in the cosmetic and flavor industry. Pristine and CO_2-expanded HKUST-1 samples with large mesopores (13–23 nm) have been reported to be highly active and selective for benzyl alcohol oxidation to benzaldehyde under mild reaction conditions.[64,65] However, the addition of a co-catalyst such as TEMPO (2,2,6,6-tetramethyl-piperidine-1-oxyl) and a base like sodium carbonate is indispensable for both studies. In the present work, the synthesized CuPd mixed-metal MOFs are employed to catalyze this reaction in the absence of these additives.

Table 1: Comparison of Catalytic Activities of Pristine HKUST-1 and CuPd Mixed-Metal MOFs for Benzyl Alcohol Oxidation after 7 h.

Catalyst	Activation Temperature (K)	Conversion (%)	Selectivity (%)
Pristine HKUST-1	423	5	99
CuPd-MOF (**1**)	423	42	95
CuPd-MOF (**2**)	no activation	51	94
	393	67	93
	423	71	92
	443	54	90
	473	49	86

The results of the catalysis test are summarized in Table 1. Pristine HKUST-1 activated at 423 K leads to only 5 % conversion at 403 K and 5 bar O_2 after 7 h, indicating the low activity of Cu^{2+}-CUS for this reaction. In comparison, CuPd-MOFs **1** and **2** activated at the same

temperature result in 42% and 71% conversion, respectively, verifying that Pd^{2+}-CUS species are the dominant active sites. The selectivity to benzaldehyde is high (> 91%), and the only side product is benzoic acid produced by overoxidation (Scheme 1). Furthermore, the influence of the catalyst activation temperature was also investigated. With increasing activation temperature to 423 K, a maximum conversion of 71% is reached, which can be attributed to more available active sites by removing pre-adsorbed species like H_2O. However, a further increase to 473 K causes a strong decrease of the conversion to 49%. Probably, the incorporation of Pd^{2+} in the metal nodes influences the thermal stability resulting in slight changes of the framework structure at higher activation temperatures (Figure S1).

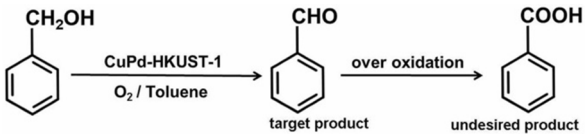

Scheme 1. Benzyl alcohol oxidation.

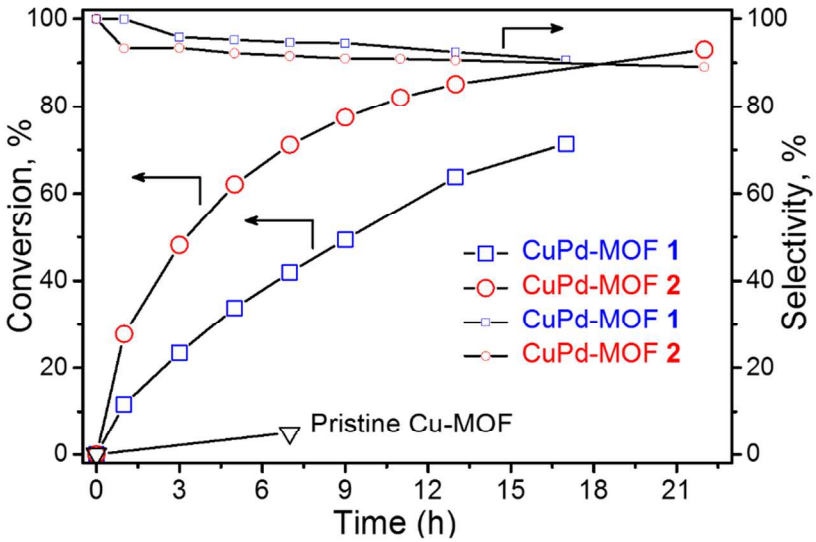

Figure 7. Conversion of benzyl alcohol and selectivity to benzaldehyde as a function of time for CuPd mixed-metal MOFs: compounds **1** (blue) and **2** (red).

As shown in Figure 7, CuPd-MOF **2** with higher Pd^{2+} doping level is the most active catalyst, leading to 93% conversion and 89% selectivity to benzaldehyde after 22 h. The oxidation of benzyl alcohol is derived to be a first-order reaction with compounds **1** and **2** (Figure S7). The reaction rate constants are calculated to amount to 0.073 and 0.140 h^{-1} for CuPd-MOFs **1** and **2,** respectively. They are proportional to the metal weight ratio of Pd^{2+} (*i.e.*, 5% and 9.73% of Pd^{2+} for compounds **1** and **2** based on EA), demonstrating again the crucial role of Pd^{2+}-CUS in this reaction.

It is worth mentioning that various Pd^{II} complexes were applied in aerobic alcohol oxidation in homogeneous catalysis,[66-68] and a catalytic cycle including the formation of a Pd^{II}alcoholate species followed by β-elimination leading to a $Pd^{II}H$ species and the formation of a $Pd^{II}OOH$ species was proposed.[66] The same reaction mechanism may also apply to the CuPd mixed-metal HKUST-1 containing highly dispersed Pd^{2+}-CUS as isolated, single active sites. Importantly, no notable difference is observed for the XRD patterns before and after reaction (see Figure S2), indicating the well-preserved structural integrity during the reaction. Overall, these results suggest a strategy to bridge homogeneous and heterogeneous catalysis.

4. CONCLUSIONS

In summary, we successfully synthesized CuPd mixed-metal HKUST-1 featuring Cu-Pd and/or Pd-Pd dimers via incorporation of Pd^{2+} into the pristine Cu-MOF by using a novel two-step synthesis. The CuPd-MOFs were characterized by a multi-technique approach including XRD, TEM-EDS, HR-XPS, and UHV-FTIRS. The results demonstrate consistently that the metal node

engineering occurs via introduction of Pd in a controlled fashion yielding mixed-metal HKUST-1 with a homogeneous distribution of Pd and Cu cations while retaining the structural integrity. These CuPd-MOFs exhibit superior activity and selectivity for the aerobic oxidation of benzyl alcohol to benzaldehyde, and the highly dispersed Pd^{2+}-CUS sites are identified as isolated single active sites. The CuPd-MOFs are also expected to be active for a variety of other aerobic oxidation reactions, in analogy to Pd^{II} complexes in numerous homogeneously catalyzed oxidation reactions. More generally, our work provides a new path to rationally design catalytically active mixed-metal MOFs in a controllable manner based on the incorporation of a second metal component exclusively at framework-nodes acting as single active sites.

ASSOCIATED CONTENT

Supporting Information. Additional TG, XRD, TEM-EDS, XPS and UHV-FTIRS analysis

AUTHOR INFORMATION

Corresponding Authors

* E-mail: baoxiang.peng@techem.rub.de (B.P.)

* E-mail: muhler@techem.rub.de (M.M.)

* E-mail: yuemin.wang@kit.edu (Y.W.)

ACKNOWLEDGMENT

The authors acknowledge financial support by the European Union's Horizon 2020 research and innovation programme under the Marie Sklodowska-Curie grant agreement No 641887 (project acronym: DEFNET). The financial support from the German Research Foundation (DFG) is also gratefully acknowledged. The authors thank Kevin Ollegott for performing the thermogravimetric measurements.

REFERENCES

(1) Murry, L. J.; Dinca, M.; Long, J. R. Hydrogen Storage in Metal–Organic Frameworks. *Chem. Soc. Rev*. **2009**, *38*, 1294-1314.

(2) Kreno, L. E.; Leong, K.; Farha, O. K.; Allendorf, M.; Van Duy-ne, R. P.; Hupp, J. T. Metal–Organic Framework Materials as Chem-ical Sensors. *Chem. Rev*. **2012**, *112*, 1105-1125.

(3) Ma, L. Q.; Abney, C.; Lin, W. B. Enantioselective Catalysis with Homochiral Metal–Organic Frameworks. *Chem. Soc. Rev*. **2009**, *38*, 1248-1256.

(4) Li, J. R.; Sculley, J.; Zhou, H.C. Metal–Organic Frameworks for Separations. *Chem. Rev*. **2012**, *112*, 869-932.

(5) Sato, H.; Kosaka, W.; Matsuda, R.; Hori, A.; Hijikata, Y.; Be-losludov, R. V.; Sakaki, S.; Takata, M.; Kitagawa, S. Self-Accelerating CO Sorption in a Soft Nanoporous Crystal. *Science* **2014**, *343*, 167-170.

(6) Zhou, H.-C.; J. R. Long, O. M. Yaghi, Introduction to Metal–Organic Frameworks. *Chem. Rev*. **2012**, *112*, 673-674.

(7) Eddaoudi, M.; Kim, J.; Rosi, N.; Vodak, D.; Wachter, J.; O'keeffe, M.; Yaghi, O. M. Systematic Design of Pore Size and Functionality in Isoreticular MOFs and Their Application in Methane Storage. *Science* **2002**, *295*, 469-472.

(8) Feng, D.; Liu, T.-F.; Su, J.; Bosch, M.; Wei, Z.; Wan, W.; Yuan, D.; Chen, Y.-P.; Wang, X.; Wang, K.; Lian, X.; Gu, Z.-Y.; Park, J.; Zou, X.; Zhou, H.-C. Stable Metal-Organic Frameworks Containing Single-Molecule Traps for Enzyme Eencapsulation. *Nat. Comm*. **2015**, *6*, 5979.

(9) Deng, H.; Grunder, S.; Cordova, K. E.; Valente, C.; Furukawa, H.; Hmadeh, M.; Gandara, F.; Whalley, A. C.; Liu, Z.; Asahina, S.; Kazumori, H.; O'keeffe, M.; Terasaki, O.; Stoddart, J. F.; Yaghi, O. M. Large-Pore Apertures in a Series of Metal-Organic Frameworks. *Science* **2012**, *336*, 1018-1023.

(10) Kim, M.; Cahill, J. F.; Su, Y. X.; Prather, K. A.; Cohen, S. M. Postsynthetic Ligand Exchange as a Route to Functionalization of 'Inert' Metal–Organic Frameworks. *Chem. Sci*. **2012**, *3*, 126-130.

(11) Li, X.; Guo, Z.; Xiao, C.; Goh, T. W.; Tesfagaber, D.; Huang, W. Tandem Catalysis by Palladium Nanoclusters Encapsulated in Metal–Organic Frameworks. *ACS Catal*. **2014**, *4*, 3490-3497.

(12) Rimoldi, M.; Howarth, A. J.; DeStefano, M. R.; Lin, L.; Goswami, S.; Li, P.; Hupp, J. T.; Farha, O. K. Catalytic Zirconium/Hafnium-Based Metal–Organic Frameworks. *ACS Catal*. **2017**, *7*, 997-1014.

(13) Yang, Q.; Xu, Q.; Jiang, H.-L. Metal-Organic Frameworks Meet Metal Nanoparticles: Synergistic Effect for Enhanced Catalysis. *Chem. Soc. Rev*. **2017**, *46*, 4774-4808.

(14) Karagiaridi, O.; Bury, W.; Tylianakis, E.; Sarjeant, A. A.; Hupp, J. T.; Farha, O. K. Opening Metal–Organic Frameworks Vol. 2: Inserting Longer Pillars into Pillared-Paddlewheel Structures through Solvent-Assisted Linker Exchange. *Chem. Mater*. **2013**, *25*, 3499-3503.

(15) Cai, G.; Jiang, H.-L. A Modulator-Induced Defect-Formation Strategy to Hierarchically Porous Metal-Organic Frameworks with High Stability. *Angew. Chem. Int. Ed*. **2017**, *56*, 563-567.

(16) Marx, S.; Kleist, W.; Baiker, A. Synthesis, Structural Properties, and Catalytic Behavior of Cu-BTC and Mixed-Linker Cu-BTC-PyDC in the Oxidation of Benzene Derivatives. *J. Catal*. **2011**, *281*, 76-87.

(17) Vermoortele, F.; Bueken, B.; Le Bars, G.; Van de Voorde B.; Vandichel, M.; Houthoofd, K.; Vimont, A.; Daturi, M.; Waroquier, M.; Van Speybroeck, V.; Kirschhock, C.; De Vos, D. E. Synthesis Modulation as a Tool to Increase the Catalytic Activity of Metal–Organic Frameworks: The Unique Case of UiO-66(Zr). *J. Am. Chem. Soc*. **2013**, *135*, 11465-11468.

(18) Wu, H.; Chua, Y. S.; Krungleviciute, V.; Tyagi, M.; Chen, P.; Yildirim, T.; Zhou, W. Unusual and Highly Tunable Missing Linker Defects in Zirconium Metal-Organic Framework UiO-66 and Their Important Effects on Gas Adsorption. *J Am. Chem. Soc.* **2013**, *135*, 10525–10532.

(19) Fang, Z.; Bueken, B.; De Vos, D. E.; Fischer, R. A. Defect-Engineered Metal-Organic Frameworks. *Angew. Chem. Int. Ed*. **2015**, *54*, 7234-7254.

(20) Fang, Z.; Dürholt, J. P.; Kauer, M.; Zhang, W.; Lochenie, C.; Jee, B.; Albada, B.; Metzler-Nolte, N.; Pöppl, A.; Weber, B.; Muhler, M.; Wang, Y.; Schmid, R.; Fischer, R. A. Structural Complexity in Metal–Organic Frameworks: Simultaneous Modification of Open Metal Sites and Hierarchical Porosity by Systematic Doping with Defective Linkers. *J. Am. Chem. Soc*, **2014,** *136*, 9627-9636.

(21) Cliffe, M. J.; Wan, W.; Zou, X. D.; Chater, P. A.; Kleppe, A. K.; Tucker, M. G.; Wilhelm, H.; Funnell, N. P.; Coudert, F. X.; Goodwin, A. L. Correlated Defect Nanoregions in a Metal-Organic Framework. *Nat. Commun*. **2014**, *5*, 4176.

(22) Barin, G.; Krungleviciute, V.; Gutov, O.; Hupp, J. T.; Yildirim, T.; Farha, O. K. Defect Creation by Linker Fragmentation in Metal–Organic Frameworks and Its Effects on Gas Uptake Properties. *Inorg. Chem*. **2014**, *53*, 6914-6919.

(23) Kozachuk, O.; Luz, I.; Llabrés i Xamena, F. X.; Noei, H.; Kauer, M.; Albada, H. B.; Bloch, E. D.; Marler, B.; Wang, Y.; Muhler, M.; Fischer, R. A. Multifunctional, Defect-Engineered Metal-Organic Frameworks with Ruthenium Centers: Sorption and Catalytic Properties. *Angew. Chem. Int. Ed*. **2014**, *53*, 7058–7062

(24) Gutov, O. V.; Hevia, M. G.; Escudero-Adan, E. C.; Shafir, A. Metal–Organic Framework (MOF) Defects under Control: Insights into the Missing Linker Sites and Their Implication in the Reactivity of Zirconium-Based Frameworks. *Inorg. Chem*. **2015**, *54*, 8396-8400.

(25) Cliffe, M. J.; Hill, J. A.; Murray, C. A.; Coudert, F.-X.; Goodwin, A. L. Defect-Dependent Colossal Negative Thermal Expansion in UiO-66(Hf) Metal–Organic Framework. *Phys. Chem. Chem. Phys*. **2015,** *17*, 11586-11592.

(26) Trickett, C. A.; Gagnon, K. J.; Lee, S.; Gandara, F.; Burgi, H. B.; Yaghi, O. M. Definitive Molecular Level Characterization of Defects in UiO-66 Crystals. *Angew. Chem. Int. Ed*. **2015**, *54*, 11162–11167.

(27) Zhang, W. H.; Kauer, M.; Halbherr, O.; Epp, K.; Guo, P. H.; Gonzalez, M. I.; Xiao, D. J.; Wiktor, C.; Llabrés i Xamena, F. X.; Wöll, C.; Wang, Y.; Muhler, M.; Fischer, R. A. Ruthenium Metal-Organic Frameworks with Different Defect Types: Influence on Porosity, Sorption, and Catalytic Properties. *Chem. Eur. J.* **2016**, *22*, 14297–14307.

(28) Canivet, J.; Vandichel, M.; Farrusseng, D. Origin of Highly Active Metal-Organic Framework Catalysts: Defects? Defects! *Dalton Trans.* **2016**, *45*, 4090–4099.

(29) Yuan, S. A.; Zou, L. F.; Qin, J. S.; Li, J. L.; Huang, L.; Feng, L. A.; Wang, X. A.; Bosch, M.; Alsalme, A.; Cagin, T.; Zhou, H. C. Construction of Hierarchically Porous Metal-Organic Frameworks Through Linker Labilization. *Nat. Commun*. **2017**, *8*, 15356.

(30) Slater, B.; Wang, Z. R.; Jiang, S. X.; Hill, M. R.; Ladewig, B. P. Missing Linker Defects in a Homochiral Metal-Organic Framework: Tuning the Chiral Separation Capacity. *J Am. Chem. Soc*. **2017**, *139*, 18322–18327.

(31) Rogge, S.M.J.; Bavykina, A.; Hajek, J.; Garcia, H.; Olivos-Suarez, A.I.; Sepulveda-Escribano, A.; Vimont, A.; Clet, G.; Bazin, P.; Kapteijn, F.; Daturi, M.; Ramos-Fernandez, E.V.; Llabrés i Xamena, F. X.; Van Speybroeck, V.; Gascon, J. Metal–Organic and Covalent Organic Frameworks as Single-Site Catalysts. *Chem. Soc. Rev.* **2017**, *46*, 3134-3184.

(32) Wang, Y.; Wöll, C. Chemical Reactions at Isolated Single-Sites Inside Metal-Organic Frameworks. *Catal. Lett*. **2018**, *148*, 2201-2222.

(33) Chui, S. S. Y.; Lo, S. M. F.; Charmant, J. P. H.; Orpen, A. G.; Williams, I. D. A Chemically Functionalizable Nanoporous Material $[Cu_3(TMA)_2(H_2O)_3]_n$. *Science* **1999**, 283, 1148–1150.

(34) Opanasenko, M.; Dhakshinamoorthy, A.; Scamzhy, M.; Nachtigall, P.; Horáček, M.; Garcia, H.; Čejka, J. Comparison of the Catalytic Activity of MOFs and Zeolites in Knoevenagel Condensation. *Catal. Sci. Technol*. **2013**, *3*, 500-507.

(34) Kumar, R. S.; Kumar, S. S.; Kulandainathan, M. A. Efficient Electrosynthesis of Highly Active Cu3(BTC)2-MOF and its Catalytic Application to Chemical Reduction. *Microporous Mesoporous Mater*. **2013**, *168*, 57-64.

(36) Schlichte, K.; Kratzke, T.; Kaskel, S. Improved Synthesis, Thermal Stability and Catalytic Properties of the Metal-Organic Framework Compound $Cu_3(BTC)_2$. *Microporous Mesoporous Mater.* **2004**, *73*, 81-88.

(37) Corma, A.; Iglesias, M.; Llabrés i Xamena, F. X.; Sanchez, F. Cu and Au Metal–Organic Frameworks Bridge the Gap between Homogeneous and Heterogeneous Catalysts for Alkene Cyclopropanation Reactions. *Chem.-Eur. J.* **2010**, *16*, 9789-9795.

(38) Luz, I.; Llabrés i Xamena, F. X.; Corma, A. Bridging Homogeneous and Heterogeneous Catalysis with MOFs: "Click" Reactions with Cu-MOF Catalysts. *J. Catal.* **2010**, *276*, 134-140.

(39) Sun, Q.; Liu, M.; Li, K.; Han, Y.; Zuo, Y.; Chai, F.; Song, C.; Zhang, G.; Guo, X. Synthesis of Fe/M (M = Mn, Co, Ni) Bimetallic Metal Organic Frameworks and Their Catalytic Activity for Phenol Degradation under Mild Conditions. *Inorg. Chem. Front*. **2017**, *4*, 144-153.

(40) Pariyar, A.; Asl, H. Y.; Choudhury, A. Tetragonal versus Hexagonal: Structure-Dependent Catalytic Activity of Co/Zn Bimetallic Metal–Organic Frameworks. *Inorg. Chem*. **2016**, *55*, 9250-9257.

(41) Wang, L.; Wu, Y.; Gao, R.; Ren, L.; Chen, M.; Feng, X.; Zhou, J.; Wang, B. Fe/Ni Metal–Organic Frameworks and Their Binder-Free Thin Films for Efficient Oxygen Evolution with Low Overpotentia. *ACS, Appl. Mater. Interfaces* **2016**, *8*, 16736-16743.

(42) Dolgopolova, E. A.; Brandt, A. J.; Ejegbavwo, O. A.; Duke, A. S.; Maddumapatabandi, T. D.; Galhenage, R. P.; Larson, B. W.; Reid, O. G.; Ammal, S. C.; Heyden, A.; Chandrashekhar, M.; Stavila, V.; Chen, D. A.; Shustova, N. B. Electronic Properties of Bimetallic Metal–Organic Frameworks (MOFs): Tailoring the Density of Electronic States through MOF Modularity. *J. Am. Chem. Soc*. **2017**, *139*, 5201-5209.

(43) Chen, Y.-Z.; Wang, C.; Wu, Z.-Y.; Xiong, Y.; Xu, Q.; Yu, S.-H.; Jiang, H.-L. From Bimetallic Metal-Organic Framework to Porous Carbon: High Surface Area and Multicomponent Active Dopants for Excellent Electrocatalysis. *Adv. Mater*. **2015**, *27*, 5010-5016.

(44) Zhai, Q.-G.; Bu, X.; Mao, C.; Zhao, X.; Feng, P. Systematic and Dramatic Tuning on Gas Sorption Performance in Heterometallic Metal–Organic Frameworks. *J. Am. Chem. Soc*. **2016**, *138*, 2524-2527.

(45) Dhakshinamoorthy, A.; Asiri, A. M.; Garcia, H. Mixed-Metal or Mixed-Linker Metal Organic Frameworks as Heterogeneous Catalysts. *Catal. Sci. Technol*. **2016**, *6*, 5238–5261.

(46) Binder, A.; Seipenbusch, M.; Muhler, M.; Kasper, G. Kinetics and Particle Size Effects in Ethene Hydrogenation over Supported Palladium Catalysts at Atmospheric Pressure. *J. Catal*. **2009**, *268*, 150-155.

(47) Wu, X. F.; Neumann, H.; Beller, M. Palladium-Catalyzed Carbonylative Coupling Reactions between Ar-X and Carbon Nucleophiles. *Chem. Soc. Rev*. *2011*, *40*, 4986-5009.

(48) Musaev, D. G.; Figg, T. M.; Kaledin, A. L. Versatile Reactivity of Pd-Catalysts: Mechanistic Features of the Mono-N-Protected Amino Acid Ligand and Cesium-Halide Base in Pd-Catalyzed C–H Bond Functionalization, *Chem. Soc. Rev*. **2014**, *43*, 5009-5031.

(49) McDonald, R. I.; Liu, G.; Stahl, S. S. Palladium(II)-Catalyzed Alkene Functionalization via Nucleopalladation: Stereochemical Pathways and Enantioselective Catalytic Applications. *Chem. Rev*. **2011**, *111*, 2981-3019.

(50) Selander, N.; Szabo, K. J. Catalysis by Palladium Pincer Complexes. *Chem. Rev.* **2011**, *111*, 2048-2076.

(51) Seechurn, C. C. C. J.; Kitching, M. O.; Colacot, T. J.; Snieckus, V. Palladium-Catalyzed Cross-Coupling: a Historical Contextual Perspective to the 2010 Nobel Prize. *Angew. Chem. Int. Ed*. **2012**, *51*, 5062-5085.

(52) Vlaar, T.; Ruijter, E.; Maes, B. U. W.; Orru, R. V. A. Palladium-Catalyzed Migratory Insertion of Isocyanides: An Emerging Platform in Cross-Coupling Chemistry, *Angew. Chem. Int. Ed*. **2013**, *52*, 7084-7097.

(53) Llabrés i Xamena, F. X.; Abad, A.; Corma, A.; Garcia, H. MOFs as Catalysts: Activity, Reusability and Shape-Selectivity of a Pd-Containing MOF. *J. Catal*. **2007**, *250*, 294-298.

(54) Zhang, W.; Chen, Z.; Al-Naji, M.; Guo, P.; Cwik, S.; Halbherr, O.; Wang, Y.; Muhler, M.; Wilde, N.; Gläser, R.; Fischer, R. A. Simultaneous Introduction of Various Palladium Active Sites into MOF via One-Pot Synthesis: Pd@$[Cu_{3-x}Pd_x(BTC)_2]_n$, *Dalton. Trans*. **2016**, *45*, 14883-14887.

(55) Wang, Y.; A. Glenz, A.; Muhler, M.; Wöll, C. A New Dualpurpose Ultrahigh Vacuum Infrared Spectroscopy Apparatus Optimized for Grazing-Incidence Reflection as well as for Transmission Geometries. *Rev. Sci. Instrum*. **2009**, *80*, 113108.

(56) Wang, Y.; Wöll, C. IR Spectroscopic Investigations of Chemical and Photochemical Reactions on Metal Oxides: Bridging the Materials Gap. *Chem. Soc. Rev*. **2017**, *46*, 1875-1932.

(57) Kim, H. K.; Yun, W. S.; Kim, M.-B.; Kim, J. Y.; Bae, Y.-S.; Lee, J.; Jeong, N. C. A Chemical Route to Activation of Open Metal Sites in the Copper-Based Metal–Organic Framework Mate-rials HKUST-1 and Cu-MOF-2. *J. Am. Chem. Soc*. **2015**, *137*, 10009-10015.

(58) Chowdhury, P.; Bikkina, C.; Meister, D.; Dreisbach, F.; Gumma, S. Comparison of Adsorption Isotherms on Cu-BTC Metal Organic Frameworks Synthesized from Different Routes. *Microporous Mesoporous Mater*. **2009**, *117*, 406-413.

(59) Liang, Z.; Marshall, M.; Chaffee, A. L. CO_2 Adsorption-Based Separation by Metal Organic Framework (Cu-BTC) versus Zeolite (13X). *Energy & Fuels* **2009**, *23*, 2785-2789.

(60) Seo, Y.-K.; Hundal, G.; Jang, I. T.; Hwang, Y. K.; Jun, C.-H.; Chang, J.-S. Microwave Synthesis of Hybrid Inorganic–Organic Materials Including Porous $Cu_3(BTC)_2$ from Cu(II)-Trimesate Mixture. *Microporous Mesoporous Mater*. **2009**, *119*, 331-337.

(61) Tan, H.-Z.; Wang, Z.-Q.; Xu, Z.-N.; Sun, J.; Chen, Z.-N.; Chen, Q.-S.; Chen, Y.; Guo, G.-C. Active Pd(II) Complexes: Enhancing Catalytic Aactivity by Ligand Effect for Carbonylation of Methyl Nitrite to Dimethyl Carbonate. *Catal. Sci. Technol*. **2017**, *7*, 3785-3790.

(62) St Petkov, P.; Vayssilov, G. N.; Liu, J. X.; Shekhah, O.; Wang, Y.; Wöll, C.; Heine, T. Defects in MOFs: a Thorough Characterization. *ChemPhysChem.* **2012**, *13*, 2025–2029.

(63) Chakarova, K.; Ivanova, E.; Hadjiivaov, K.; Klissurski, D.; Knözinger, H. Co-Ordination Chemistry of Palladium Cations in Pd-H-ZSM-5 as Revealed by FTIR Spectra of Adsorbed and Coadsorbed Probe Molecules (CO and NO). *Phys. Chem. Chem. Phys.* **2004**, *6*, 3702-3709.

(64) Dhakshinamoorthy, A.; Alvaro, M.; Garcia, H. Aerobic Oxidation of Benzylic Alcohols Catalyzed by Metal−Organic Frameworks Assisted by TEMPO. *ACS Catal.* **2011**, *1*, 48-53.

(65) Peng, L.; Zhang, J.; Xue, Z.; Han, B.; Sang, X.; Liu, C.; Yang, G. Highly Mesoporous Metal–Organic Framework Assembled in a Switchable Solvent. *Nat. Commun*. **2014**, *5*, 4465.

(66) Nishimura, T.; Onoue, T.; Ohe, K.; Uemura, S. Palladium(II)-Catalyzed Oxidation of Alcohols to Aldehydes and Ketones by Molecular Oxygen. *J. Org. Chem*. **1999**, *64*, 6750-6755.

(67) Stahl, S. S. Palladium Oxidase Catalysis: Selective Oxidation of Organic Chemicals by Direct Dioxygen-Coupled Turnover. *Angew. Chem., Int. Ed*. **2004**, *43*, 3400–3420.

(68) Sigman, M. S.; Jensen, D. R. Ligand-Modulated Palladium-Catalyzed Aerobic Alcohol Oxidations. *Acc. Chem. Res*. **2006**, *39*, 221–229.

TOC Graphic:

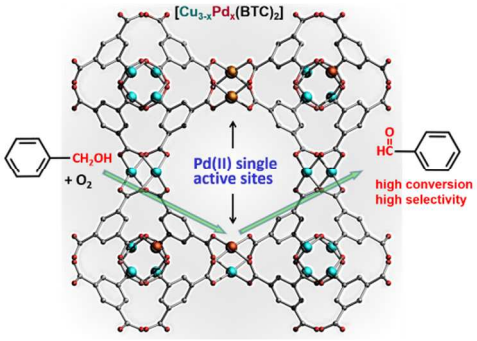
[Cu3-xPdx(BTC)2]
CH2OH
+ O2
Pd(II) single
active sites
O
HC
high conversion
high selectivity